

Limits of SNR and Practical Consequences

Klaas P. Pruessmann, PhD

Institute for Biomedical Engineering, ETH Zurich, 8092 Zurich, Switzerland

All MR data, whether raw signals, images, or spectra, are inevitably contaminated by noise that is picked up during data acquisition. The ratio of the useful MR signal component and the noise level, i.e. the signal-to-noise ratio (SNR), is a key quality criterion for MR data sets. SNR requirements vary for different applications. Often an SNR on the order of 50 will be sufficient, while at SNRs below 10 many types of data are nearly useless.

MR signals are inherently weak, so ensuring sufficient SNR is a concern for every MR experiment. Potentially excessive SNR can usually be converted into other benefits, such as higher spatial resolution, shorter scan time, and artifact reduction. Therefore, maximizing the basic SNR yield is always a central objective. In doing so there are many factors and parameters to consider, ranging from the baseline field strength B_0 to the receiver hardware, image parameters, and sequence design. However, even with ideal hardware and optimal parameters the SNR yield will always remain limited.

In the following, we study the physics that determine the noise and signal levels, means for improving and controlling the SNR, and the inherent limits imposed by the underlying electrodynamics.

Thermal noise: origin and characterization

In MR practice the notion of noise is sometimes used in a fairly broad sense, including fluctuations in the MR signal, reconstruction errors and artifacts of all sorts. In order to explore the limits of the SNR, however, we will use a more rigid definition of noise, encompassing only genuine stochastic, thermal fluctuations of the signal voltage.

The cause of this fundamental type of noise is the thermal agitation of electric charges. Such charges exist everywhere in the experimental setup: in the sample to be imaged, in the receiver coil, including its circuitry, insulation and housing, and also in the entire environment. Highly mobile electrons abound in metals, e.g. in the coil conductor. Large amounts of positive and negative ions are present in live tissues and even dipolar molecules, such as water, contribute to thermal noise.

The density and mobility of charges in each material is comprehensively described by its conductivity, which is frequency-dependent. At the relatively low frequencies used in in-vivo MR (typically on the order of 100 MHz) conduction in the relevant materials is largely due to single charges such as electrons and ions.

Thermally moving charges contaminate the MR signal by electromagnetic interaction with the signal detector. The standard mode of MR detection is Faraday induction in a resonant receiver coil. The relevant signal is the positive circularly polarized component of the voltage at the output of the detector circuit. Hence, more specifically, the relevant thermal noise is the corresponding component of the fluctuating voltage that moving charges generate at the detector terminals. Conceptually speaking it reflects the coupling between the thermal degrees of freedom of the whole setup and the electrical parameters of the detector terminals.

The noise voltage U_N results from stochastic motion, hence it is itself random in nature and cannot be predicted. Yet its statistics can be readily characterized. Due to the stochastic nature of the underlying motion and the linearity of the electromagnetic coupling the noise voltage has a zero-mean Gaussian distribution. Hence it can be fully characterized by its mean square or, statistically speaking, its variance

$$\Psi = \overline{|U_N|^2}, \quad [1]$$

where the bar indicates temporal averaging. The noise level is the standard deviation of U_N and given by the square root of Ψ .

Quantifying thermal noise

Quantifying thermal noise is straightforward experimentally. Using Eq. [1] its variance can be readily obtained from a sufficiently large set of voltage samples taken at the detector output in the absence of MR signal.

However, for minimizing noise and for studying the limits thereof it is important to consider theoretically how the noise variance depends on the coil design and the experimental setup in general. To do so, in principle one must characterize all parts of the setup thermodynamically and establish their electromagnetic coupling with the coil terminals.

This is demanding to do in a forward fashion. However, it can be done quite elegantly using the so-called principle of reciprocity (1-3). Broadly speaking, the approach is based on the observation that the thermoelectric coupling between the setup and the coil terminals works both ways. So, instead of analyzing the generation of voltage by thermal motion one can as well study the generation of thermal motion by an external voltage applied to the coil terminals.

To implement this idea we perform a thought experiment in which the coil circuit is used in transmission mode rather than for signal reception. At its terminals we apply an alternating voltage of frequency ω and suitable amplitude such that it drives a given reference current I_0 (e.g. 1 mA) into the coil circuit. Throughout the coil, the sample, and their environment the voltage and current will generate spatially varying electric and magnetic fields $\mathbf{E}(\omega, \mathbf{r})$, $\mathbf{H}(\omega, \mathbf{r})$. Note that these field vectors have complex entries, reflecting both the amplitude and the phase of the field components, which equally oscillate at the frequency ω .

For the generation of thermal energy via electric charges only the electric field $\mathbf{E}(\omega, \mathbf{r})$ is relevant. In conjunction with the local conductivity $\sigma(\omega, \mathbf{r})$ it causes currents with the density

$$\mathbf{j}(\omega, \mathbf{r}) = \sigma(\omega, \mathbf{r}) \mathbf{E}(\omega, \mathbf{r}) \quad [2]$$

These currents dissipate power, converting electrical energy into thermal energy. The power dissipated in the volume element dV at the position \mathbf{r} reads

$$dP(\omega, \mathbf{r}) = \mathbf{j}(\omega, \mathbf{r}) \cdot \mathbf{E}(\omega, \mathbf{r}) dV = \sigma(\omega, \mathbf{r}) |\mathbf{E}(\omega, \mathbf{r})|^2 dV \quad [3]$$

Viewing the dissipation as an ohmic loss it can be rewritten as

$$dP(\omega, \mathbf{r}) = dR(\omega, \mathbf{r}) I_0^2 \quad , \quad [4]$$

where

$$dR(\omega, \mathbf{r}) = \frac{1}{I_0^2} \sigma(\omega, \mathbf{r}) |\mathbf{E}(\omega, \mathbf{r})|^2 dV \quad [5]$$

is the contribution of dV to the overall resistance. Here it is important to note that dR does not depend on the reference current because $\mathbf{E}(\omega, \mathbf{r})$, $\mathbf{H}(\omega, \mathbf{r})$ scale with I_0 .

The power dissipated in this hypothetical experiment is the desired measure of thermoelectric coupling that can now be used to determine the noise voltage in the receive mode.

Of course, in addition to the coupling coefficient, the noise voltage also depends on the available thermal energy. Incorporating this factor, the contribution of the volume element dV to the total noise variance reads

$$d\Psi(\omega, \mathbf{r}) = \frac{k_B T(\mathbf{r})}{\pi I_0^2} dP(\omega, \mathbf{r}) d\omega \quad , \quad [6]$$

where k_B denotes the Boltzmann constant and $T(\mathbf{r})$ the local absolute temperature. This equation illustrates that the noise variance is additive, just like the dissipated power. This means that every volume element makes an individual noise contribution and the total variance is simply the sum of these contributions. In terms of statistics it means that noise from different positions is independent and uncorrelated. The same holds for the spectral dimension. Thermal noise at any two different frequencies is uncorrelated. Hence in a frequency band between ω_1 and ω_2 we will find noise with a total variance of

$$\Psi = \frac{k_B}{\pi I_0^2} \int_V \int_{\omega_1}^{\omega_2} T(\mathbf{r}) \sigma(\omega, \mathbf{r}) |\mathbf{E}(\omega, \mathbf{r})|^2 d\omega dV, \quad [7]$$

where V denotes a sufficiently large volume, comprising the experimental setup and surrounding space where $\mathbf{E}(\omega, \mathbf{r})$ is significant. In MR the relevant frequency bandwidth is usually much smaller than the Larmor frequency ω and $\sigma(\omega, \mathbf{r})$, $\mathbf{E}(\omega, \mathbf{r})$ are practically constant within this band. Defining the bandwidth $BW = (\omega_2 - \omega_1)/2\pi$, Eq. [7] can hence be simplified to

$$\Psi = \frac{2BW k_B}{I_0^2} \int_V T(\mathbf{r}) \sigma(\omega, \mathbf{r}) |\mathbf{E}(\omega, \mathbf{r})|^2 dV \quad [8]$$

Using the analogy of ohmic resistance given in Eq. [5], this equation can be further simplified to

$$\Psi = 2BW k_B \int_V T(\mathbf{r}) dR(\omega, \mathbf{r}). \quad [9]$$

Some further insight can be gained by considering that the temperatures of the sample and the coil circuit are approximately constant. Writing the integral separately for the sample, the circuit and the remaining environment we obtain

$$\Psi = 2BW k_B T_C R_C(\omega) + 2BW k_B T_S R_S(\omega) + 2BW k_B \int_{V_E} T(\mathbf{r}) dR(\omega, \mathbf{r}) \quad [10]$$

where T_C , T_S and R_C , R_S denote the temperatures and total effective resistances of the circuit and the sample, respectively, and V_E denotes the environment volume. For the circuit and sample contributions we have now arrived at the familiar formula for Johnson noise of a resistor, as derived by J.B. Johnson and H. Nyquist (4, 5). Note that Eq. [10] differs from their original formulation by a factor of 2, which is due to the fact that we consider only the positive circularly polarized noise component.

In common MR applications with $\omega/2\pi$ on the order of 100 MHz and efficient receiver coils, the sample noise is usually dominant. However, circuit noise can become significant with small coils and at lower frequencies (6). Noise from the environment can often be neglected. However, it may become relevant at very high frequencies where propagating RF components gain in significance.

Noise covariance of coil arrays

So far we have considered signal detection with a single receiver coil. Arrays of multiple receiver coils are frequently used for enhancing the signal-to-noise ratio (SNR) (7) and for parallel imaging with enhanced encoding speed (8-13). In this case each coil has its individual noise variance, which can be calculated as described above. However, the multiple-coil situation is a bit more complicated because noise from different coils can be correlated. The correlation can be accounted for by generalizing the scalar variance Ψ to an $n_C \times n_C$ noise covariance matrix, where n_C denotes the number of coils involved. Its entries are given by a generalized form of Eq. [8]:

$$\Psi_{ij} = \overline{U_{N,i} U_{N,j}^*} = \frac{2BW k_B}{I_0^2} \int_V T(\mathbf{r}) \sigma(\omega, \mathbf{r}) \mathbf{E}_i(\omega, \mathbf{r}) \cdot \mathbf{E}_j^*(\omega, \mathbf{r}) dV, \quad [11]$$

where \mathbf{E}_i , \mathbf{E}_j denote the electric transmit fields of the coils i , j , respectively. For $i = j$ Eq. [11] is equivalent to Eq. [8]. Hence the diagonal entries of the covariance matrix are the familiar single-coil noise variances, which are always real numbers. The off-diagonal elements ($i \neq j$) represent the noise correlation between the coils i , j . They are generally complex because correlated noise components can exhibit relative phase shifts.

Equation 11 confirms the intuition that noise from a given volume element can contribute to noise correlation between two coils if it couples with both of their terminals. Nevertheless, the contributions will still be uncorrelated when the electric transmit fields of the two coils are orthogonal at the respective position.

The equation also illustrates that correlated noise can stem from anywhere in the setup, from the sample, the circuitry, and the environment. Significant noise correlation can occur in particular among coils that couple

directly, e.g. inductively. This is because coupling in the transmit mode causes the coils to generate common electric field components, which give rise to correlated noise contributions from across the entire setup.

Following the same derivation as for the single-coil case, the noise covariance of a coil array can be equivalently viewed as arising from ohmic resistances, involving the notion of mutual resistance R_{ij} (7).

Reducing thermal noise

The options for minimizing thermal noise can be summarized by studying the variable factors that determine the noise variance and covariance according to Eqs. [8] and [11], respectively.

First, the bandwidth is an obvious handle on the noise level. Reducing the bandwidth reduces the noise variance proportionally. However it also decreases the efficiency of spatial signal encoding, with the bandwidth proportional to k-space speed. As a result the acquisition time grows as the square of the inverse noise level. Hence the factor BW permits mitigating noise only at the expense of scan speed (14).

The temperature factor offers somewhat more freedom. Adjusting it is truly practical only for receiver coils and their circuitry and housing. Nevertheless, here cooling is actually a feasible and effective option (6,15).

The remaining factors are the conductivity, $\sigma(\omega, \mathbf{r})$, and the electric transmit field, $\mathbf{E}(\omega, \mathbf{r})$. The role of the conductivity is ambiguous, which is best understood in the transmission picture. Remember that the input voltage and hence the electric field $\mathbf{E}(\omega, \mathbf{r})$ are scaled such that they drive the net reference current I_0 between the coil terminals. Hence, broadly speaking, one can distinguish ‘favorable’ currents, which actually contribute to the net current and ‘adverse’ eddy currents, which close on themselves and only contribute to dissipation.

Clearly, the coil conductor should be highly conductive, forming the direct pathway for ‘favorable’ currents. This may seem paradoxical because the integrand in Eqs. [8], [11] is proportional to the conductivity. However, it is important to note that the electric transmit field implicitly depends on the conductivity. Enhancing the coil’s conductivity reduces the electric field inside it and hence overall reduces the noise integral. For high conductivity at room temperature copper and silver are preferred conductor materials. Additionally their conductivity can be enhanced again by cooling (6,15). The ultimate in conductivity is offered by superconductor materials (16-18), which however require extreme cooling and are much more difficult to handle than copper and silver.

In the sample the conductivity plays a different role. Here the primary current in the coil generates mainly magnetic field, which per se hardly causes dissipation. However its oscillation causes electric eddy fields, which give rise to ‘adverse’ currents that scale with the local conductivity. Hence, contrary to the coil conductor, conductivity in the object generally increases the thermal noise. So in principle it would be very desirable to reduce the sample’s conductivity, which however is usually not an option. Alternatively one can aim to minimize the electric eddy fields in the sample. However, as discussed later on, this approach is quite limited, too, because the underlying magnetic fields determine the coil’s sensitivity to the MR signal.

For the environment similar considerations hold as for the sample. Here, too, conductivity is mainly adverse and difficult to manipulate. The key difference is that both magnetic and electric transmit fields can be freely minimized in the environment, because MR sensitivity is not an issue there.

In summary, there are limited means of enhancing the SNR by mitigating thermal noise. Noise contributions from coils and circuitry and from the environment can be addressed by technical measures. However, little can be done to control thermal noise that originates within the sample. In this respect, sample noise is the most fundamental.

Sensitivity to MR signal

In (nuclear) MRI and MRS the magnetic resonance signal stems from magnetic moments associated with the spin of atomic nuclei. So the signal sources are of magnetic nature, which distinguishes them fundamentally from the electric noise sources. As a consequence, the signal sensitivity of a receiver coil is associated with its magnetic rather than electric transmit field.

Let $\mathbf{H}(\omega, \mathbf{r})$ denote the magnetic field that the coil generates in our thought experiment, i.e. when driven with a reference current I_0 of frequency ω . Then the nuclear magnetic moment of a voxel with volume ΔV at the position \mathbf{r} , precessing at the frequency ω , induces the signal voltage (1, 3)

$$U_s = \frac{M(\mathbf{r}) \Delta V \mu(\mathbf{r}) \omega}{I_0} (H_x(\omega, \mathbf{r}) - iH_y(\omega, \mathbf{r})), \quad [12]$$

where $M(\mathbf{r})$ denotes the local transverse magnetization, $\mu(\mathbf{r})$ denotes the local magnetic permeability and $H_x(\omega, \mathbf{r})$, $H_y(\omega, \mathbf{r})$ are the magnetic field components in the x and y direction, z being the direction of the static field B_0 .

Image SNR

In standard Fourier MRI with a single coil, a certain number of signal samples are acquired and then subject to Fourier transform for reconstruction. For each image pixel the Fourier transform coherently averages the signal contributions from the corresponding voxel, while cancelling those of all other voxels. In this process, the concomitant noise is averaged, too, but incoherently because it is uncorrelated between different data samples. As a consequence, the image SNR grows as the square root of the number of samples:

$$\text{SNR}(\mathbf{r}) = \sqrt{N_{\text{Samples}}} \frac{|U_s(\mathbf{r})|}{\sqrt{\Psi}}. \quad [13]$$

However, unfortunately this does not mean that more data samples necessarily yield an image with higher SNR. Expanding U_s , Ψ according to Eqs. [8, 12] we obtain

$$\text{SNR}(\mathbf{r}) = \sqrt{N_{\text{Samples}}} M(\mathbf{r}) \Delta V \omega \frac{\mu(\mathbf{r}) |H_x(\omega, \mathbf{r}) - iH_y(\omega, \mathbf{r})|}{\sqrt{2k_B BW \int_V T(\mathbf{r}) \sigma(\omega, \mathbf{r}) |\mathbf{E}(\omega, \mathbf{r})|^2 dV}}, \quad [14]$$

reminding us to keep an eye also on the voxel volume ΔV . For instance, resolving more pixels in a given FOV reduces ΔV , reducing the SNR faster than it grows with the number of signal samples. Therefore images with higher resolution usually have lower SNR, despite requiring more data samples and more scan time. When isotropic resolution is desired, the voxel volume decreases even as the cube of the voxel diameter, resulting in an even more rapid SNR decay. Hence, for preventing critically low image SNR the choice of the resolution and slice thickness is especially important.

Another important factor in Eq. [14] is, of course, the available transverse magnetization $M(\mathbf{r})$, which itself depends on many parameters, such as the spin density and polarization, the relaxation times, the type of imaging sequence and its timing, the flip angles used etc. The most straightforward means of maximizing $M(\mathbf{r})$ is the sequence design. Other ways of boosting it include contrast agents, the use of hyperpolarization, and increasing B_0 . The latter additionally enhances the signal frequency ω , which also helps the SNR according to Eq. [14]. However, enhancing the frequency incurs changes also in the electrostatics, leading to some compensation of the SNR benefit by a concomitant increase in the noise level.

The simplest means of improving the SNR, finally, is repeating a scan multiple times and averaging the results. In terms of Eq. [14] this approach corresponds to enhancing the overall number of signal samples (N_{Samples}), while leaving all other factors unchanged. Hence the SNR grows as the square root of the number of scan repetitions.

Ultimate intrinsic SNR

For a given sample, field strength B_0 , and experimental protocol only the receiver coil(s) and circuitry and the electrodynamic properties of the environment remain to be optimized. As discussed above there are means that, in principle, permit reducing the noise contributions from coil circuits and environment to an insignificant level. Then only the magnetic and electric transmit fields inside the sample remain for SNR optimization. Generally, the magnetic transmit field $\mathbf{H}(\omega, \mathbf{r})$ is to be maximized, while minimizing the electric field $\mathbf{E}(\omega, \mathbf{r})$. The laws of electrostatics offer infinitely many degrees of freedom for this joint optimization. So one might hope that they could permit extracting arbitrarily high SNR with ideal coil arrays. However, this is not the case because the two types of fields are connected too closely. As mentioned earlier, all magnetic field in the sample gives rise to electric eddy fields. More generally, the magnetic and electric fields are coupled by Maxwell's equations.

The limiting role of Maxwell's equations can be explored by another thought experiment, assuming that any physically realizable coil or set of coils was available and all but sample noise was successfully suppressed. In this fashion the ultimate intrinsic SNR (19-21) can be determined for a given imaging task. Selected results of such a study (21) are shown in Figs. 1, 2. As the sample a spherical object was assumed with material properties similar to those encountered in live brain tissue.

Figure 1 shows the ultimate SNR in the transverse plane for sphere sizes between 10 cm and 50 cm and B_0 between 1 T and 10 T. Obviously the ultimate SNR is finite and depends strongly on the field strength and the position within the sphere. It increases with B_0 and towards the sphere's surface. In particular, the minimum of the ultimate SNR is always located in the center of the sphere.

Figure 2 focuses on the dependence of the ultimate SNR upon the field strength B_0 . It shows double-logarithmic plots of the ultimate SNR for B_0 ranging from 0.5 T to 12 T. Three different positions in the central transverse plane were investigated for several sphere sizes. For the plots in the upper row, the conductivity was maintained at average in-vivo brain values, whereas for the lower plots approximately lossless conditions ($\sigma=10^{-5} (\Omega\text{m})^{-1}$) were assumed for comparison. All plots are approximately linear for low B_0 , with nearly unit slope, corresponding to linear growth of the ultimate SNR with B_0 . For the peripheral position ($r_0=0.95*\text{FOV}/2$), this behavior persists throughout the entire B_0 range. For the other, deeper positions, a transition to a second regime with greater slope, hence higher power growth, is observed. The transition generally occurs sooner for larger objects/FOVs and deeper target positions.

The two types of SNR behavior correspond to the fact that the behavior of RF fields differs fundamentally for different ranges of distance from their source. The near field is dominated by evanescent field components, which are of high amplitude but decay rapidly with distance. The extent of the near-field zone is roughly equal to the RF wavelength, which is inversely proportional to B_0 . Hence, MR detection is near-field dominated at low B_0 or from positions close to the object's surface. In the intermediate and far-field zone propagating field components become more relevant. Permitting field focusing, the propagating components lead to enhanced growth of the ultimate SNR at high B_0 and from positions far away from the surface. This benefit is compromised by conduction in the sample, as illustrated by comparing with the nearly lossless case.

References

- (1) Hoult DI, Richards RE. The Signal-to-Noise Ratio of the Nuclear Magnetic Resonance Experiment. *J Magn Reson* 1976;24:71-85.
- (2) Insko EK, Elliott MA, Schotland JC, Leigh JS. Generalized reciprocity. *J Magn Reson* 1998;131(1):111-117.
- (3) Hoult DI. The Principle of Reciprocity in Signal Strength Calculations - A Mathematical Guide. *Concepts Magn Reson* 2000;12(4):173-187.
- (4) Johnson JB. Thermal Agitation of Electricity in Conductors. *Phys Rev* 1928;32:97-109.
- (5) Nyquist H. Thermal Agitation of Electric Charge in Conductors. *Phys Rev* 1928;32:110-113.
- (6) Ginefri JC, Darrasse L, Crozat P. High-temperature superconducting surface coil for in vivo microimaging of the human skin. *Magnetic Resonance in Medicine* 2001;45(3):376-382.
- (7) Roemer PB, Edelstein WA, Hayes CE, Souza SP, Mueller OM, The NMR phased array. *Magnetic Resonance in Medicine* 1990;16:192-225.
- (8) Carlson JW. An Algorithm for NMR Imaging Reconstruction Based on Multiple RF Receiver Coils. *Journal of Magnetic Resonance* 1987;74(2):376-380.
- (9) Hutchinson M, Raff U. Fast MRI Data Acquisition Using Multiple Detectors. *Magnetic Resonance in Medicine* 1988;6(1):87-91.
- (10) Ra JB, Rim CY. Fast Imaging Using Subencoding Data Sets from Multiple Detectors. *Magnetic Resonance in Medicine* 1993;30(1):142-145.
- (11) Sodickson DK, Manning WJ. Simultaneous acquisition of spatial harmonics (SMASH): Fast imaging with radiofrequency coil arrays. *Magnetic Resonance in Medicine* 1997;38(4):591-603.
- (12) Pruessmann KP, Weiger M, Scheidegger MB, Boesiger P. SENSE: Sensitivity encoding for fast MRI. *Magnetic Resonance in Medicine* 1999;42(5):952-962.

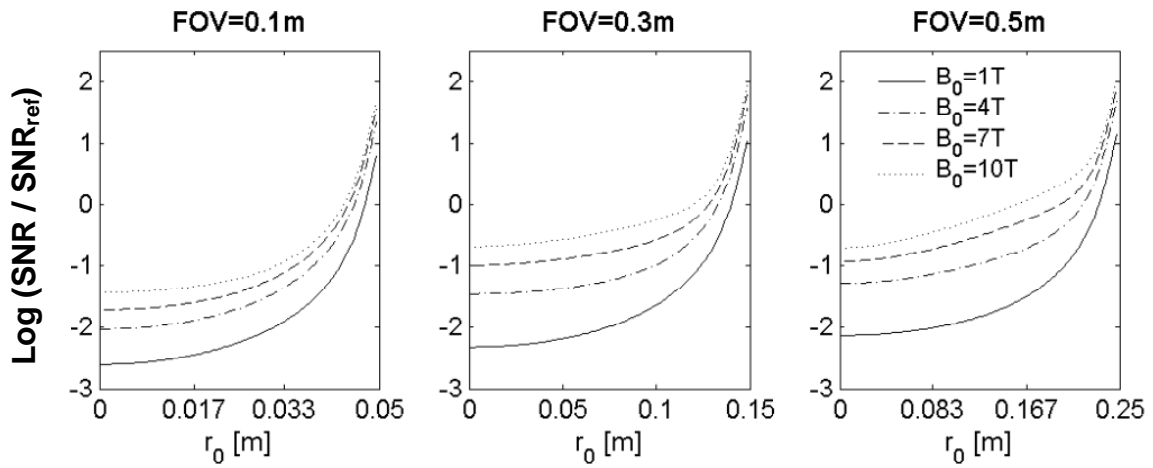


Fig. 1 Ultimate intrinsic SNR, relative to a constant reference value SNR_{ref} . The three different fields of view (FOV) correspond to equally large spherical samples. r_0 denotes the distance from the center of the sphere within the transverse plane.

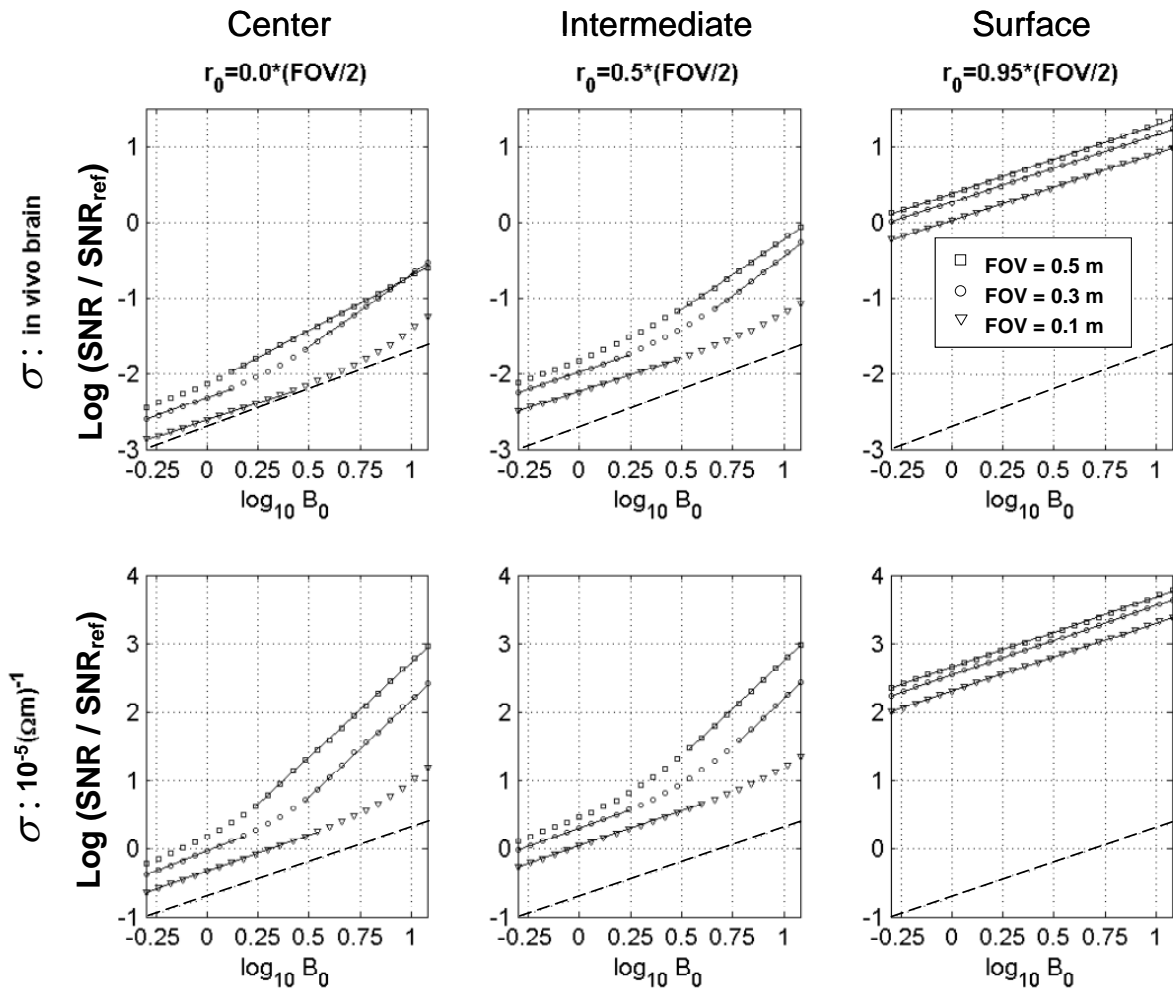


Fig. 2 Ultimate intrinsic SNR, relative to a constant reference value SNR_{ref} . Different fields of view (FOV) correspond to equally large spherical samples. r_0 denotes the distance from the center of the sphere within the transverse plane. The dashed lines show a unit slope, corresponding to linear SNR growth, for comparison.

References continued

- (13) Griswold MA, Jakob PM, Heidemann RM, Nittka M, Jellus V, Wang JM, Kiefer B, Haase A. Generalized Autocalibrating Partially Parallel Acquisitions (GRAPPA). *Magnetic Resonance in Medicine* 2002;47(6):1202-1210.
- (14) Macovski A. Noise in MRI. *Magnetic Resonance in Medicine* 1996;36:494-497.
- (15) Wright AC, Song HK, Wehrli FW. In vivo MR micro imaging with conventional radiofrequency coils cooled to 77 degrees K. *Magnetic Resonance in Medicine* 2000;43(2):163-169.
- (16) Vanheteren JG, James TW, Bourne LC. Thin-Film High-Temperature Superconducting Rf Coils for Low-Field Mri. *Magnetic Resonance in Medicine* 1994;32(3):396-400.
- (17) Black RD, Early TA, Roemer PB, Mueller OM, Mogrocampero A, Turner LG, Johnson GA. A High-Temperature Superconducting Receiver for Nuclear-Magnetic-Resonance Microscopy. *Science* 1993;259(5096):793-795.
- (18) Hall AS, Alford NM, Button TW, Gilderdale DJ, Gehring KA, Young IR. Use of High-Temperature Superconductor in a Receiver Coil for Magnetic-Resonance-Imaging. *Magnetic Resonance in Medicine* 1991;20(2):340-343.
- (19) Ocali O, Atalar E. Ultimate intrinsic signal-to-noise ratio in MRI. *Magn Reson Med* 1998;39(3):462-473.
- (20) Ohliger MA, Grant AK, Sodickson DK. Ultimate intrinsic signal-to-noise ratio for parallel MRI: electromagnetic field considerations. *Magn Reson Med* 2003;50(5):1018-1030.
- (21) Wiesinger F, Boesiger P, Pruessmann KP. Electrodynamics and Ultimate SNR in Parallel MR Imaging. *Magn Reson Med* 2004;52(2):376-390.